






Determination of $^{57}\text{Co}(n, xp)$ cross sections using the surrogate reaction ratio method

Ramandeep Gandhi ^{1,2,*} S. Santra ^{1,2,†} A. Pal ^{1,2} B. K. Nayak^{1,2} P. C. Rout^{1,2} D. Chattopadhyay^{1,2,‡} A. Kundu^{1,2}
A. Baishya ^{1,2} T. Santhosh ^{1,2} S. K. Pandit¹ G. Mohanto¹ and A. Diaz-Torres³

¹Nuclear Physics Division, Bhabha Atomic Research Centre, Mumbai 400085, India

²Homi Bhabha National Institute, Anushaktinagar, Mumbai 400094, India

³Department of Physics, University of Surrey, Guildford, Surrey GU2 7XH, United Kingdom



(Received 1 April 2022; revised 8 July 2022; accepted 8 September 2022; published 23 September 2022)

The compound nuclei $^{58}\text{Co}^*$ and $^{61}\text{Ni}^*$ have been populated at overlapping excitation energies by transfer reactions $^{56}\text{Fe}(^6\text{Li}, \alpha)^{58}\text{Co}^*$ (surrogate of $n + ^{57}\text{Co}$) at $E_{\text{lab}} = 35.9$ MeV and $^{59}\text{Co}(^6\text{Li}, \alpha)^{61}\text{Ni}^*$ (surrogate of $n + ^{60}\text{Ni}$) at $E_{\text{lab}} = 40.5$ MeV, respectively. The $^{57}\text{Co}(n, xp)$ cross sections in the equivalent neutron energy range of 8.6–18.8 MeV have been determined within the framework of surrogate reaction ratio method using $^{60}\text{Ni}(n, xp)$ cross section values from the literature as reference. The proton decay probabilities of the compound systems have been determined by measuring evaporated protons at backward angles in coincidence with projectile-like fragments detected around the grazing angle. The measured $^{57}\text{Co}(n, xp)$ cross sections are in good agreement with both the predictions of TALYS-1.8 statistical model code with default parameters using different microscopic level densities and data evaluation library JEFF-3.3 up to equivalent neutron energy ≈ 12.6 MeV, while for higher energies the measured $^{57}\text{Co}(n, xp)$ cross sections are found to be consistently higher than the predictions. However, the TALYS-1.8 calculations with modified values of input potential parameters provide a reasonable reproduction of the measured $^{57}\text{Co}(n, xp)$ cross sections for the entire neutron energy range. The observed discrepancies at higher energies between the experimental data and the predictions of both the JEFF-3.3 library and the TALYS-1.8 calculations with default parameters indicate the need of new evaluations for this reaction.

DOI: 10.1103/PhysRevC.106.034609

I. INTRODUCTION

Neutron-induced reaction cross sections data are most important for design and technology development of advance reactors. The accuracy of these cross sections decides the safety assessment of nuclear energy production. The presence of neutron energy spectra above the traditional limits of fission reactors, for accelerator driven systems and fusion reactors open up larger number of threshold reaction channels such as $(n, 2n)$, (n, p) , (n, α) , (n, np) , (n, d) , $(n, 3n)$, and $(n, n\alpha)$ reactions. The highly energetic and intense neutron flux produced via D + T reaction in fusion reactors cause various reactions on structural material (stainless steel). These incident neutrons cause atomic displacements within the materials, leading to the generation and accumulation of radiation defects which modifies the physical properties of the structural materials. Perhaps, (n, xp) and $(n, x\alpha)$ reactions are more problematic since they produce gaseous elements such as hydrogen (H) and helium (He), leading to swelling and embrittlement of structural material of the reactor. Additionally, this high-intensity neutron flux will produce many short- and long-lived radionuclides by transmutation reactions with the

elements in the initial stainless steel composition (Fe, Ni, Mn, Cr, Co, and Nb). $^{53}\text{Mn}(T_{1/2} = 3.74 \times 10^6 \text{ yr})$, $^{54}\text{Mn}(T_{1/2} = 312.3 \text{ d})$, $^{55}\text{Fe}(T_{1/2} = 2.73 \text{ yr})$, $^{60}\text{Fe}(T_{1/2} = 1.5 \times 10^6 \text{ yr})$, $^{57}\text{Co}(T_{1/2} = 271.79 \text{ d})$, $^{58}\text{Co}(T_{1/2} = 70.86 \text{ d})$, $^{60}\text{Co}(T_{1/2} = 5.27 \text{ yr})$, $^{59}\text{Ni}(T_{1/2} = 7.6 \times 10^4 \text{ yr})$, and $^{63}\text{Ni}(T_{1/2} = 100.1 \text{ yr})$ are some of unstable nuclei produced in mass region 50–60. For safety assessment and understanding overall neutronics of fusion reactors, experimental data on (n, xp) and $(n, x\alpha)$ cross sections with the above radionuclides are of crucial importance [1–4].

^{57}Co is one of the important radionuclides produced during the operation of a fusion reactor, predominantly via $^{58}\text{Ni}(n, np)$, $^{58}\text{Ni}(n, d)$, and $^{58}\text{Ni}(n, 2n)^{57}\text{Ni}(\beta^+)$ reactions having neutron threshold energies of 8.31, 6.05, and 12.4 MeV, respectively, as depicted in Fig. 1. Since Ni constitutes ≈ 10 –14% of SS composition, the intense flux of high energy neutrons in fusion reactor will lead to significant growth of ^{57}Co [5–7]. Since $^{57}\text{Co}(n, p)$ and $^{57}\text{Co}(n, \alpha)$ are exothermic reactions with respective Q values of 1.619 and 1.858 MeV, ^{57}Co will contribute to production of hydrogen and helium via (n, xp) and $(n, x\alpha)$ reactions. Therefore it is of utmost importance to determine the cross section for hydrogen and helium production via $^{57}\text{Co}(n, xp)$ and $^{57}\text{Co}(n, x\alpha)$ reactions.

^{57}Co is a short-lived isotope of $T_{1/2} = 271.79 \text{ d}$, formed specifically in reactor operational conditions. Due to the unavailability of the ^{57}Co target, direct measurements of $^{57}\text{Co}(n, xp)$ and $^{57}\text{Co}(n, x\alpha)$ cross sections are challenging. Taking advantage of surrogate reaction ratio method, as used

*ramangandhipu@gmail.com

†ssantra@barc.gov.in

‡Current address: Faculty of Science and Technology (Physics), ICFAI University Tripura, Agartala 799210, India.

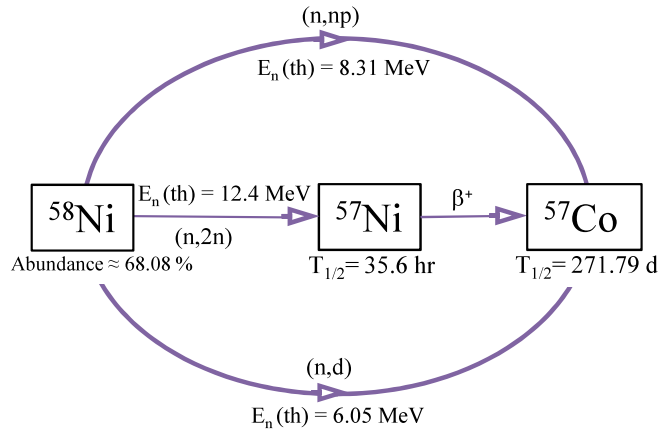


FIG. 1. Major pathways of ^{57}Co production in a typical fusion reactor.

in our earlier works [8–10], we attempt to determine the cross sections for the $^{57}\text{Co}(n, xp)$ reaction.

In the present work, the $^{56}\text{Fe}(^6\text{Li}, \alpha)^{58}\text{Co}^*$ transfer reaction has been used as a surrogate of $n + ^{57}\text{Co}$ reaction to determine the $^{57}\text{Co}(n, xp)$ reaction cross sections. The $^{60}\text{Ni}(n, xp)$ reaction cross sections have been used as a reference by populating $^{61}\text{Ni}^*$ compound system through $^{59}\text{Co}(^6\text{Li}, \alpha)^{61}\text{Ni}^*$ transfer reaction at similar excitation energies. The identification of projectile-like fragment (PLF) α in transfer reactions $^{56}\text{Fe}(^6\text{Li}, \alpha)^{58}\text{Co}^*$ and $^{59}\text{Co}(^6\text{Li}, \alpha)^{61}\text{Ni}^*$ confirm the formation of compound systems $^{58}\text{Co}^*$ and $^{61}\text{Ni}^*$, respectively. The evaporated protons at backward angles are measured in coincidence with the PLF α around grazing angle to determine the proton decay probabilities of compound systems $^{58}\text{Co}^*$ and $^{61}\text{Ni}^*$. The ratios of these proton decay probabilities are multiplied with the ratios of neutron-induced compound nuclear formation cross sections ($\sigma_{n+^{57}\text{Co}}^{\text{CN}}$ and $\sigma_{n+^{60}\text{Ni}}^{\text{CN}}$) at corresponding excitation energy bins. This provides the ratios of the compound nuclear reaction cross sections [i.e., $\sigma^{57\text{Co}(n, xp)}$ to $\sigma^{60\text{Ni}(n, xp)}$] as a function of excitation energy. They are further multiplied by known $^{60}\text{Ni}(n, xp)$ reaction cross sections to obtain the desired $^{57}\text{Co}(n, xp)$ reaction cross sections. The paper has been organized as follows. The key features of the experimental setup and data analysis are given in Sec. II. Results and discussions are given in Sec. III, followed by the summary and conclusions in Sec. IV.

II. EXPERIMENTAL DETAILS AND DATA ANALYSIS

Freshly prepared self-supporting target of natural Fe (abundance $^{56}\text{Fe} \approx 92\%$) of thickness $\approx 700 \mu\text{g}/\text{cm}^2$ and ^{59}Co (abundance $\approx 100\%$) of thickness $\approx 500 \mu\text{g}/\text{cm}^2$ were bombarded by ^6Li beams of energies $E_{\text{lab}} = 35.9$ and 40.5 MeV, respectively, at BARC-TIFR Pelletron Accelerator Facility in Mumbai. For the present experiment, the surrogate reactions of interest, their ground-state Q values (Q_{gg}), the compound nuclei (CN) formed, neutron separation energies (S_n), and corresponding equivalent neutron-induced reactions are listed in Table I.

TABLE I. Surrogate reactions investigated in the present experiment, their ground-state Q values (Q_{gg}), the CN formed, neutron separation energies (S_n), and corresponding equivalent neutron-induced reactions.

$E_{\text{beam}}^{^6\text{Li}}$ (MeV)	Surrogate reaction	Q_{gg} (MeV)	CN	S_n (MeV)	Equivalent neutron-induced reaction
35.9	$^{56}\text{Fe}(^6\text{Li}, \alpha)^{58}\text{Co}^*$	10.90	$^{58}\text{Co}^*$	8.573	$^{57}\text{Co}(n, xp)$
40.5	$^{59}\text{Co}(^6\text{Li}, \alpha)^{61}\text{Ni}^*$	13.65	$^{61}\text{Ni}^*$	7.820	$^{60}\text{Ni}(n, xp)$

The schematic diagram of the experimental setup is shown in Fig. 2, which is also described in Ref. [10]. The PLFs were identified by silicon surface barrier (SSB) $\Delta E - E$ detector telescope (T) mounted at 25° with respect to the beam direction, around the grazing angle. The SSB telescope consisted of ΔE and E detector of thicknesses $\approx 150 \mu\text{m}$ and 1 mm, respectively. A typical two-dimensional energy calibrated plot of ΔE versus E_{total} (total energy) clearly identifies different PLFs like proton, deuteron, triton, and α particles as shown in Fig. 3(a). The typical energy resolution of the SSB telescope was ≈ 150 keV.

The evaporated particles (e.g., p , d , t , and α) from the compound nuclei $^{58}\text{Co}^*$ and $^{61}\text{Ni}^*$ in coincidence with the PLF(α), were detected by two large area Si strip detector telescopes (S1 and S2) mounted at backward angles (120° and 150°) with respect to beam direction. Each position sensitive Si strip telescope had angular opening of $\approx 16^\circ$ and consisted of a ΔE detector of thickness $\approx 60 \mu\text{m}$ and an E detector of thickness of $\approx 1500 \mu\text{m}$. Each strip detector of strip telescope S1 and S2 had 16 vertical strips of size $3.1 \text{ mm} \times 50 \text{ mm}$ covering an active area of $50 \text{ mm} \times 50 \text{ mm}$. Figure 3(b) shows a typical two-dimensional energy calibrated spectrum of ΔE versus E_{total} , acquired in one of the 16 $\Delta E - E$ strip combinations of Si strip detector telescopes S1, which clearly

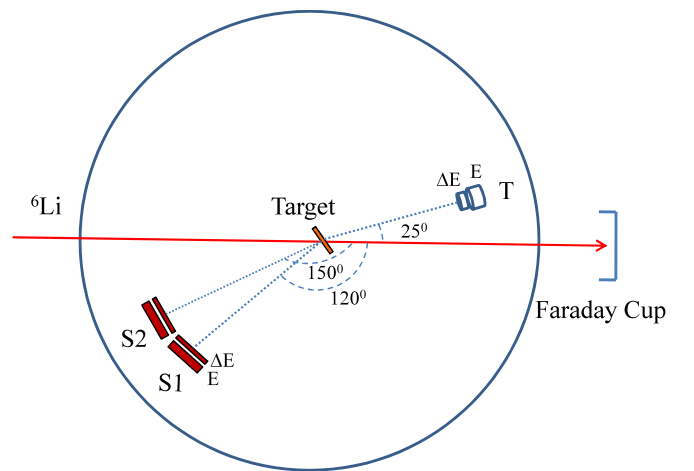


FIG. 2. A schematic diagram of experimental setup inside a 1.5-m-diameter scattering chamber. Here T is a silicon surface barrier (SSB) detector telescope for detecting the PLFs placed at a distance of 17 cm from the target center. The Si strip telescopes S1 and S2 (placed at 21 cm from the target center) have been used to identify the evaporated particles like p , d , t , and α at backward angles.

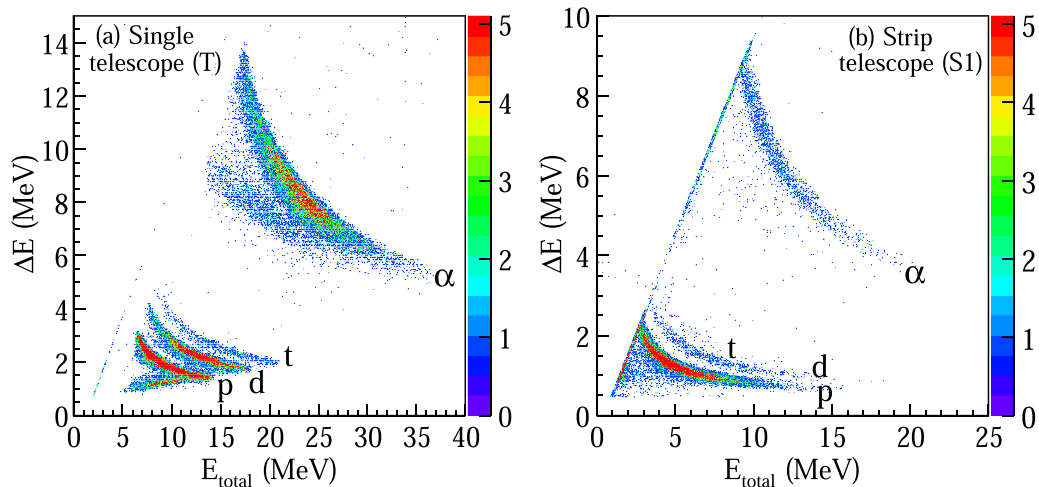


FIG. 3. (a) A typical correlation plot of ΔE versus E_{total} (total energy) corresponding to the particles detected in Si surface barrier detector telescope (T) placed at 25° for the ${}^6\text{Li} + {}^{56}\text{Fe}$ reaction at $E_{\text{lab}} = 35.9$ MeV. (b) A typical plot of ΔE versus E_{total} (total energy) obtained from one of the 16 ΔE - E strip combinations of Si strip detector telescope S1 placed at 120° for the ${}^6\text{Li} + {}^{56}\text{Fe}$ reaction at $E_{\text{lab}} = 35.9$ MeV.

identifies the particles of H isotopes (p , d , t) and ${}^4\text{He}$. Typical energy resolution of a strip detector was ≈ 100 keV.

By measuring the ${}^{12}\text{C}({}^6\text{Li}, d){}^{16}\text{O}^*$ reaction at $E_{\text{lab}} = 20$ MeV and using the known excited states of ${}^{16}\text{O}^*$ formed, the energy calibration of the SSB telescope (T) and strip telescopes (S1 and S2) have been made. Energy calibration was also done by the known energies of α particles from a Pu-Am α source and found to be consistent. The time correlations between the projectile-like particles detected in the T detector and the corresponding decay particles (from the residual target) detected in detector S1 or S2 were recorded by time to amplitude converter (TAC). Figure 4 shows a typical two-dimensional plot of energy of α particle (E_α) detected in telescope T versus TAC between the particles detected in T and evaporated protons detected in S1 for ${}^6\text{Li} + {}^{56}\text{Fe}$ reaction at $E_{\text{lab}} = 35.9$ MeV.

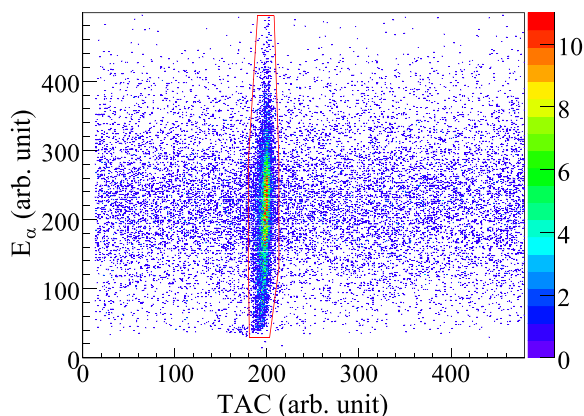


FIG. 4. A typical two-dimensional plot of energy of α particle (E_α) detected in telescope T versus the TAC (time correlation) between the α particles detected in the single telescope T and the evaporated protons detected in the strip detector telescope S1 for ${}^6\text{Li} + {}^{56}\text{Fe}$ reaction measured at $E_{\text{lab}} = 35.9$ MeV.

Two-body kinematics is employed for PLF α channel to obtain the excitation energy spectra of targetlike compound systems of ${}^{58}\text{Co}^*$ and ${}^{61}\text{Ni}^*$ through the “event-by-event analysis.” The excitation energy spectra obtained for ${}^{58}\text{Co}^*$ and ${}^{61}\text{Ni}^*$ compound nuclei in coincidence with evaporated protons are shown in Figs. 5(a) and 5(b), respectively. The respective excitation energy spectra corresponding to the singles PLF (α) are shown in Figs. 5(c) and 5(d). Energy bin of 0.5 MeV is used to generate each of these spectra. The compound systems ${}^{58}\text{Co}^*$ and ${}^{61}\text{Ni}^*$ are found to be populated at overlapping excitation energies in the range of ≈ 17 – 27 MeV, as shown by dotted lines in Fig. 5.

The proton decay (particle evaporation) probabilities from ${}^{58}\text{Co}^*$ and ${}^{61}\text{Ni}^*$ compound nuclei produced in the transfer reactions are obtained using the following relation:

$$P_p^{\text{CN}}(E^*) = \frac{N_{\alpha,p}(E^*)}{N_\alpha(E^*)}. \quad (1)$$

N_α and $N_{\alpha,p}$ denotes the singles (α) and coincidence counts (between PLF α and evaporated p), obtained corresponding to excitation energy (E^*).

The evaporation nature of emitted protons from compound nuclei ${}^{58}\text{Co}^*$ has been confirmed by comparing the proton spectrum with the statistical model code PACE4 [11] predictions at excitation energy, $E^* = 22$ MeV as shown in Fig. 6. The experimental proton spectrum compare well with the predictions of PACE4 calculations, confirming proton evaporation from the compound system ${}^{58}\text{Co}^*$. Additionally, an isotropic distribution of evaporated protons in the center of mass (by S1 and S2 detector telescopes) in the angular range $\approx 110^\circ$ – 160° , in coincidence with PLF(α) is also observed in the present study, which is again confirmatory signature of evaporation.

The proton decay probabilities $P_p^{{}^{58}\text{Co}}(E^*)$ and $P_p^{{}^{61}\text{Ni}}(E^*)$ of the excited compound systems ${}^{58}\text{Co}^*$ and ${}^{61}\text{Ni}^*$, formed in transfer reactions ${}^{56}\text{Fe}({}^6\text{Li}, \alpha)$ and ${}^{59}\text{Co}({}^6\text{Li}, \alpha)$ at respective beams energies of 35.9 and 40.5 MeV corresponding to the desired and reference reactions, have been determined in steps

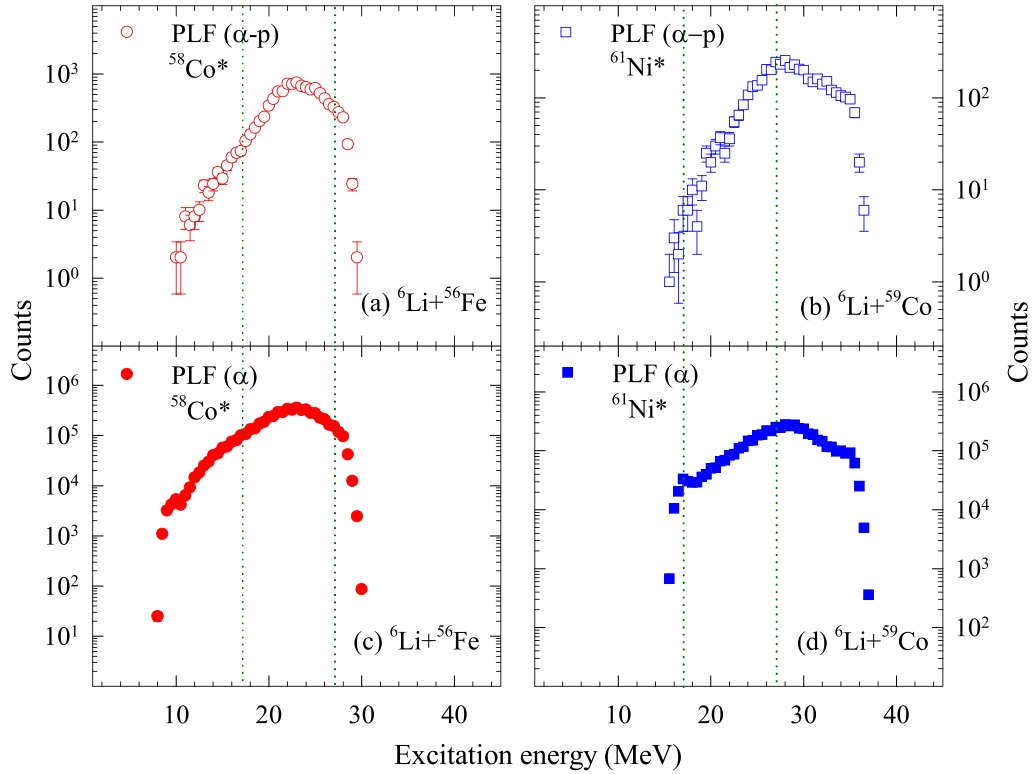


FIG. 5. Excitation energy spectra of the targetlike fragments produced in ${}^6\text{Li} + {}^{56}\text{Fe}$ and ${}^6\text{Li} + {}^{59}\text{Co}$ reactions corresponding to PLF α with [(a) and (b)] and without [(c) and (d)] coincidence with evaporated protons. Overlapping excitation energy regions marked between two dotted lines are used for determining the desired cross sections.

of 1.0-MeV excitation energy bins using Eq. (1) and the results are shown in Fig. 7. The ratio of the compound nuclear reaction cross sections $\sigma^{57}\text{Co}(n, xp)$ and $\sigma^{60}\text{Ni}(n, xp)$ has been obtained at the same excitation energy using the following

relation:

$$\frac{\sigma^{57}\text{Co}(n, xp)(E^*)}{\sigma^{60}\text{Ni}(n, xp)(E^*)} = \frac{\sigma_{n+57\text{Co}}^{\text{CN}}(E^*) P_p^{58\text{Co}}(E^*)}{\sigma_{n+60\text{Ni}}^{\text{CN}}(E^*) P_p^{61\text{Ni}}(E^*)}, \quad (2)$$

The reference reaction ${}^{60}\text{Ni}(n, xp)$ cross sections ($\sigma^{60}\text{Ni}(n, xp)$) as a function of excitation energy are

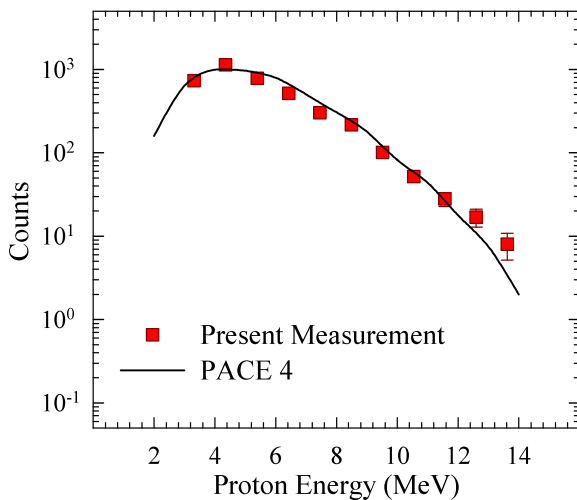


FIG. 6. Measured proton energy spectrum in coincidence with PLF α particles for the ${}^6\text{Li} + {}^{56}\text{Fe}$ reaction at $E_{\text{lab}} = 35.9$ MeV corresponding to a compound nucleus excitation energy of ≈ 22 MeV. The prediction by the statistical model code PACE4, normalized to the data, is shown as a continuous line.

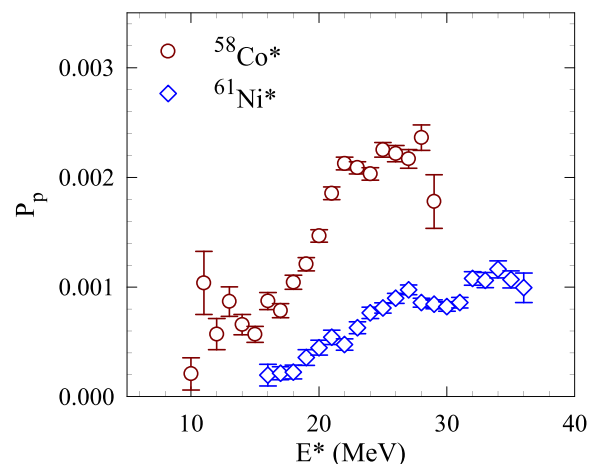


FIG. 7. The proton decay probabilities $P_p(E^*)$ as a function of excitation energy (E^*) for the excited compound systems ${}^{58}\text{Co}^*$ and ${}^{61}\text{Ni}^*$ formed in transfer reactions ${}^{56}\text{Fe}({}^6\text{Li}, \alpha)$ and ${}^{59}\text{Co}({}^6\text{Li}, \alpha)$ at ${}^6\text{Li}$ beams of energies $E_{\text{lab}} = 35.9$ and 40.5 MeV, respectively.

taken from JENDL-4.0 [12] evaluation that closely reproduces the available experimental data taken from EXFOR [13], as shown in Fig. 11 of Ref. [9]. Thus, the uncertainties in the cross sections of the reference reaction $^{60}\text{Ni}(n, xp)$ have not been considered while determining the cross sections for the desired $^{57}\text{Co}(n, xp)$ reaction. The neutron capture cross sections leading to compound systems $^{58}\text{Co}^*$ and $^{61}\text{Ni}^*$ ($\sigma_{n+^{57}\text{Co}}^{\text{CN}}$ and $\sigma_{n+^{60}\text{Ni}}^{\text{CN}}$) are calculated by using TALYS-1.8 [14] statistical model code in the excitation energy range $E^* = 17\text{--}27$ MeV. The calculated neutron capture cross sections along with the measured proton decay probabilities for compound systems $^{58}\text{Co}^*$ and $^{61}\text{Ni}^*$, and the reference reaction $^{60}\text{Ni}(n, xp)$ cross sections have been used to determine $^{57}\text{Co}(n, xp)$ reaction cross sections over excitation energy range, $E^* = 17\text{--}27$ MeV in steps of 1.0 MeV excitation energy bin. The excitation energy range was then converted to equivalent neutron energy range of $E_n = 8.6\text{--}18.8$ MeV, using the expression $E_n = \frac{A+1}{A}(E^* - S_n)$, where $A+1 (=58)$ is the mass number and $S_n (=8.573$ MeV) is the neutron separation energy of the compound nucleus ^{58}Co . The cross sections for $^{57}\text{Co}(n, xp)$ reaction have been determined as a function of equivalent neutron energy as discussed in the following section.

It is important to verify the validity of the surrogate ratio method (SRM) which is applied here to determine the desired (n, xp) cross sections. It may be mentioned that Chiba *et al.* [15,16] suggest that the surrogate ratio method can be employed to determine neutron-induced fission and capture cross sections if (1) the spin distributions in two compound nuclei populated by two surrogate reactions used in the SRM are equivalent, (2) the difference of the representative spin values between the neutron-induced and surrogate reactions is not much larger than $10\hbar$, and (3) the weak Weisskopf-Ewing condition on J^π -by- J^π convergence of the branching ratios are satisfied. To check these three conditions, detailed calculations have been carried out for the present systems as described in the Appendix and it was found that the SRM approach is valid to determine the desired (n, xp) cross sections.

TABLE II. The measured proton decay probabilities $P_p(E^*)$ for the compound nuclei (CN) $^{58}\text{Co}^*$ and $^{61}\text{Ni}^*$ formed in the transfer reactions $^{56}\text{Fe}(^6\text{Li}, \alpha)$ and $^{59}\text{Co}(^6\text{Li}, \alpha)$, corresponding calculated neutron capture cross sections leading to CN $^{58}\text{Co}^*$ and $^{61}\text{Ni}^*$ ($\sigma_{n+^{57}\text{Co}}^{\text{CN}}$ and $\sigma_{n+^{60}\text{Ni}}^{\text{CN}}$), the cross sections for the reference reaction $^{60}\text{Ni}(n, xp)$, the desired $^{57}\text{Co}(n, xp)$ cross sections that are deduced using Eq. (2) at each excitation energy (E^*) bin, and equivalent neutron energy (E_n) for CN $^{58}\text{Co}^*$ corresponding to each E^* bin.

E^* (MeV)	$\sigma_{n+^{57}\text{Co}}^{\text{CN}}$ (mb)	$\sigma_{n+^{60}\text{Ni}}^{\text{CN}}$ (mb)	$P_p^{58\text{Co}}(E^*)$	$P_p^{61\text{Ni}}(E^*)$	$\sigma^{60\text{Ni}(n, xp)}$ (barn)	$\sigma^{57\text{Co}(n, xp)}$ (barn)	$E_n(\equiv n+^{57}\text{Co})$ (MeV)
17	1301.2	1320.4	0.00079	0.00021	0.09	0.35±0.10	8.6±0.5
18	1239.4	1268.9	0.00104	0.00022	0.12	0.53±0.15	9.6±0.5
19	1179	1213.9	0.00121	0.00036	0.14	0.48±0.10	10.6±0.5
20	1116	1156.1	0.00147	0.00045	0.20	0.64±0.10	11.6±0.5
21	1051.4	1096.6	0.00185	0.00054	0.26	0.87±0.11	12.6±0.5
22	987.4	1037.7	0.00206	0.00046	0.31	1.31±0.15	13.7±0.5
23	923.9	982.2	0.00209	0.00063	0.34	1.08±0.10	14.7±0.5
24	864.8	928.6	0.00203	0.00076	0.38	0.95±0.07	15.7±0.5
25	809.6	876.7	0.00225	0.00081	0.42	1.08±0.07	16.7±0.5
26	758.2	826.7	0.00222	0.00090	0.45	1.03±0.06	17.7±0.5
27	708	777.7	0.00217	0.00097	0.49	0.98±0.06	18.8±0.5

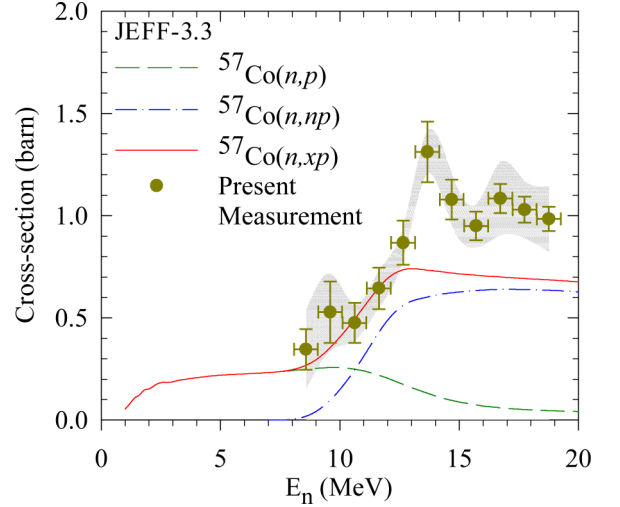


FIG. 8. The experimental cross sections for $^{57}\text{Co}(n, xp)$ reactions obtained from the surrogate ratio method have been plotted as a function of equivalent or incident neutron energy (E_n) as shown by filled circles. The gray shaded band represent additional uncertainty in the central value of the determined cross sections due to theoretical systematic uncertainties inherent to surrogate ratio method. The lines represent the predictions for the cross sections of $^{57}\text{Co}(n, p)$, $^{57}\text{Co}(n, np)$, and $^{57}\text{Co}(n, xp)$ reactions obtained from JEFF-3.3 evaluation.

III. RESULTS AND DISCUSSIONS

Using Eq. (2) and following the surrogate ratio method described above, the cross sections for $^{57}\text{Co}(n, xp)$ reaction have been determined and the results are shown as filled circles in Fig. 8. The error bars on the cross sections shown in the figure include only the statistical errors, and the error bars on equivalent neutron energies correspond to the width of the energy bins of 1.0 MeV. Table II contains the numerical values of the following quantities which are relevant to the above figure: (i) the measured proton decay probabilities $P_p(E^*)$ for

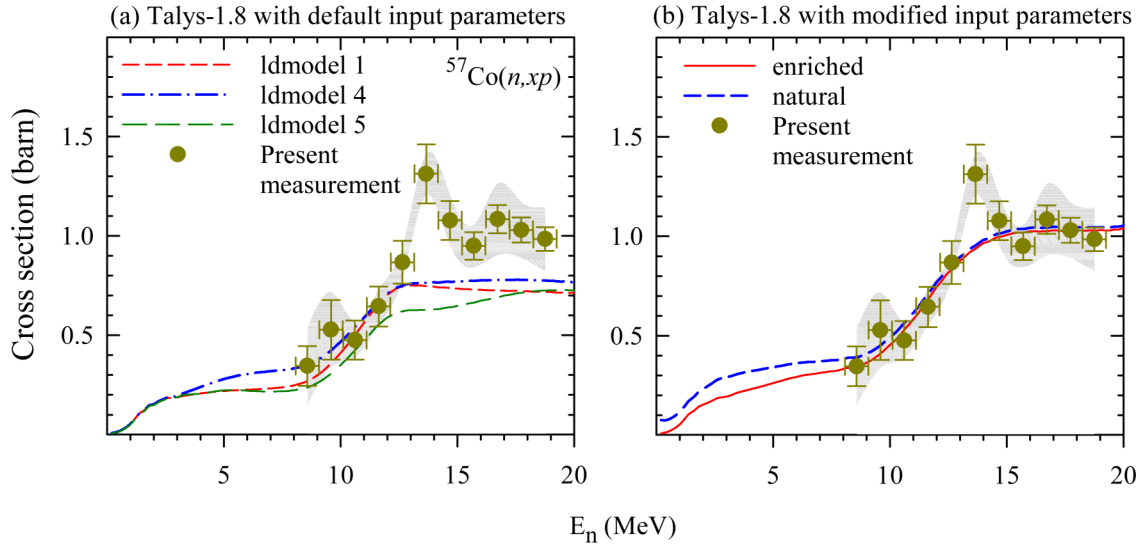


FIG. 9. (a) The experimental cross sections for $^{57}\text{Co}(n, xp)$ reactions as a function of equivalent or incident neutron energy (E_n) have been compared with TALYS-1.8 predictions with default potential parameters using different level density models (see text). (b) The experimental cross sections for $^{57}\text{Co}(n, xp)$ reactions as a function E_n have been compared with TALYS-1.8 statistical model calculations with modified input potential parameters for two cases: (i) Enriched and (ii) natural targets (see text). The level density model with “ldmodel 4” option has been chosen to obtain the best reproduction of the present measurements at all energies.

the compound nuclei (CN) $^{58}\text{Co}^*$ and $^{61}\text{Ni}^*$ formed in the transfer reactions $^{56}\text{Fe}(^6\text{Li}, \alpha)$ and $^{59}\text{Co}(^6\text{Li}, \alpha)$, (ii) corresponding calculated neutron capture cross sections leading to CN $^{58}\text{Co}^*$ and $^{61}\text{Ni}^*$ ($\sigma_{n+^{57}\text{Co}}^{\text{CN}}$ and $\sigma_{n+^{60}\text{Ni}}^{\text{CN}}$), (iii) the cross sections for the reference reaction $^{60}\text{Ni}(n, xp)$, (iv) the desired $^{57}\text{Co}(n, xp)$ cross sections that are deduced using Eq. (2) at each excitation energy (E^*) bin, and (v) the equivalent neutron energy (E_n) for CN $^{58}\text{Co}^*$ corresponding to each E^* bin. The experimental systematic uncertainties are much smaller than the error bars shown in these figures. The advantage of the surrogate ratio method is that most of the systematic errors on cross sections that may arise from detector efficiency, flux normalization, etc., reduce significantly while taking their ratios. The systematic errors in the equivalent neutron energies due to the uncertainties in beam energy, target thickness, kinematic broadening, etc., are found to be much smaller than the width of each energy bin.

However, there are theoretical systematic uncertainties inherent to the application of the SRM to determine the $^{57}\text{Co}(n, xp)$ reaction cross sections that arise mainly due to the deviation in J^π -by- J^π convergence of the branching ratios. In order to determine the theoretical systematic uncertainty corresponding to each data point, we have calculated the deviation in J dependence of the decay probability ratios [$P_{xp}^{58\text{Co}}(E^*)/P_{xp}^{61\text{Ni}}(E^*)$] corresponding to the surrogate reactions from that of n -induced reactions. The statistical model code PACE4 has been used to perform these calculations at the excitation energies $E^* = 17$ – 27 MeV, in steps of 1 MeV. It is observed that the above deviation is of the order of 8–19% for the excitation energy range $E^* = 19$ – 27 MeV. Hence SRM may be used to determine the desired reaction cross sections to the above accuracy for the excitation energy range $E^* = 19$ – 27 MeV (i.e., equivalent neutron energy range $E_n = 10.6$ – 18.8

MeV). However, for data points below $E^* = 19$ MeV ($E_n = 10.6$ MeV) there are substantial deviations (up to $\approx 56\%$) in convergence leading to large systematic errors where the weak Weisskopf-Ewing condition may not be satisfied. The theoretical systematic uncertainties determined above are represented by gray shaded regions around the experimental data points in Figs. 8 and 9.

The experimental $^{57}\text{Co}(n, xp)$ cross sections have been compared with those obtained from an evaluation data library JEFF-3.3 [17], as shown in Fig. 8. The $^{57}\text{Co}(n, p)$, $^{57}\text{Co}(n, np)$, and $^{57}\text{Co}(n, 2p)$ reactions with energy thresholds of 0.0, 6.134, and 9.099 MeV are possible sources of proton emission contributing to the total $^{57}\text{Co}(n, xp)$ cross section in the measured excitation energy region. The individual cross sections for two dominating reaction channels $^{57}\text{Co}(n, p)$ and $^{57}\text{Co}(n, np)$, evaluated using JEFF-3.3, have been shown as single-dashed (dark green) and double-dashed (blue) lines, respectively. The cross sections for $^{57}\text{Co}(n, 2p)$ proton emission channel are found to be negligibly small for incident neutron energies up to 20 MeV (not shown in the figure). The $^{57}\text{Co}(n, xp)$ cross sections from JEFF-3.3 evaluation are found to be in good agreement with present measurements up to the equivalent neutron energy ≈ 12.6 MeV, whereas for higher energies the experimental cross section values are higher than the JEFF-3.3 predictions.

Next we have tried to understand the $^{57}\text{Co}(n, xp)$ cross sections quantitatively by carrying out statistical model calculations. The statistical model code TALYS-1.8 has been employed to calculate $^{57}\text{Co}(n, xp)$ cross sections for neutron energy up to 20 MeV within the framework of Hauser-Feshbach statistical model [18]. The key input parameters required in the calculations such as nuclear masses, ground-state deformations, discrete energy levels, γ -ray strength functions, transmission coefficients, and nuclear level

densities of nuclides involved are taken from the Reference Input Parameter Library RIPL-3 [19]. The global optical model potentials for neutron and proton proposed by Koning and Delaroche [20] have been used to calculate the transmission coefficients. The TALYS-1.8 code predictions with default parameters for $^{57}\text{Co}(n, xp)$ reaction cross sections for various level density options are shown in Fig. 9(a), along with the present experimental data for a comparison. In TALYS-1.8 calculations, there are different options available for level densities of the nuclei involved in a reaction. Three options “ldmodel 1, 2, and 3” correspond to three phenomenological level density models. i.e., (i) constant temperature + Fermi gas model [21], (ii) back-shifted Fermi gas model [22], and (iii) generalized superfluid model [23], respectively. Two more options, i.e., “ldmodel 4” and “ldmodel 5” correspond to the microscopic level densities obtained from (i) Goriely’s tables [24] and (ii) Hilaire’s combinatorial tables [25], respectively. The calculated $^{57}\text{Co}(n, xp)$ reaction cross sections using “ldmodel 2 and 3,” being very close to that using “ldmodel 5,” are not shown in Fig. 9(a). It has been found that the $^{57}\text{Co}(n, xp)$ cross sections predicted by TALYS-1.8 code using the default optical model potential parameters and any one of the level density parameter options from “ldmodel 1 to ldmodel 5” compare reasonably well with experimental data for equivalent neutron energy (E_n) up to ≈ 12.6 MeV. But for $E_n > 12.6$ MeV, the TALYS-1.8 predictions are found to underestimate the experimental data. To explain the present data at all energies, the input optical model potential parameters to the TALYS-1.8 code corresponding to the neutron interaction are required to be modified. The radius parameters r_v and r_w corresponding to the real and imaginary components of the volume-central potential seen by incident neutron are increased to 1.798 and 2.157 fm from their default values of 1.199 and 1.199 fm, respectively. The depth parameter w_2 corresponding to the imaginary component of the volume-central potential has been increased from its default value of 80 to 85.6 MeV. The TALYS-1.8 calculations with modified input potential parameters and using “ldmodel 4” option, as shown by the solid curve in Fig. 9(b) are found to be in good agreement with the experimental data at all energies except the lone data point at 13.6 MeV whose value is much larger than the prediction. In all the TALYS-1.8 calculations of the present study, the discrete level densities of the initial as well as final-state nuclei have been considered by using the option “disctable 2” that corresponds to the experimental level densities available in the RIPL database.

The calculated $^{57}\text{Co}(n, xp)$ cross sections using TALYS-1.8 with modified input potential parameters for enriched target (100% ^{56}Fe) and natural Fe target are shown respectively as solid and dashed lines in Fig. 9(b). Natural Fe target has the abundances of ^{54}Fe ($\approx 5.85\%$), ^{56}Fe ($\approx 91.75\%$), ^{57}Fe ($\approx 2.12\%$), and ^{58}Fe ($\approx 0.28\%$), leading to the contributions from $^{55}\text{Co}(n, xp)$, $^{57}\text{Co}(n, xp)$, $^{58}\text{Co}(n, xp)$, and $^{59}\text{Co}(n, xp)$ reactions, respectively. The TALYS-1.8 calculations have been performed to evaluate the (n, xp) cross sections corresponding to each isotope. Finally, the cross sections are added with the weight factors equal to their abundance in natural target to obtain the cross sections for a natural target (dashed line). The cross sections for an enriched target (solid line) is obtained

from TALYS-1.8 considering only $^{57}\text{Co}(n, xp)$ reaction cross sections which corresponds to 100% enriched ^{56}Fe target. The difference in the results of (n, xp) cross sections obtained using natural Fe and enriched (^{56}Fe) targets is estimated to be maximum up to 11% in the neutron energy range of present measurements. The calculated values of $^{57}\text{Co}(n, xp)$ cross sections using TALYS-1.8 for both the enriched (100% ^{56}Fe) and natural Fe targets are in good agreement with the present data within the experimental uncertainties.

IV. SUMMARY AND CONCLUSION

In summary, we have determined the $^{57}\text{Co}(n, xp)$ cross sections by employing the surrogate reaction ratio method. The $^{58}\text{Co}^*$ and $^{61}\text{Ni}^*$ compound systems which are the surrogates of $n + ^{57}\text{Co}$ and $n + ^{60}\text{Ni}$ reactions are populated by transfer reactions $^{56}\text{Fe}(^6\text{Li}, \alpha)^{58}\text{Co}^*$ and $^{59}\text{Co}(^6\text{Li}, \alpha)^{61}\text{Ni}^*$, respectively. The compound systems $^{58}\text{Co}^*$ and $^{61}\text{Ni}^*$ are populated at overlapping excitation energies and the proton decay probabilities are measured in the excitation energy range of 17–27 MeV for both the compound systems. The $^{57}\text{Co}(n, xp)$ cross sections in the equivalent neutron energy of 8.6–18.8 MeV have been determined within the framework of surrogate reaction ratio method using $^{60}\text{Ni}(n, xp)$ cross sections as the reference. Present measurements of $^{57}\text{Co}(n, xp)$ cross sections have been compared with the predictions of TALYS-1.8 statistical model code and available data evaluation library JEFF-3.3. The experimental cross sections compare reasonably well with the predictions of both the TALYS-1.8 code with default parameters and the data evaluation library JEFF-3.3 up to $E_n \approx 12.6$ MeV, whereas for $E_n > 12.6$ MeV, the present data are found to be consistently higher than both the predictions. However, by adjusting the input potential parameter for neutron-nucleus interactions into the TALYS-1.8 code, the calculated cross sections are observed to be in very good agreement with the experimental data over the entire energy range of our interest. The present study leads to a conclusion that new evaluations may be necessary to explain the discrepancies at higher energies between the experimental data and the predictions from both the TALYS-1.8 calculations with default parameters and the JEFF-3.3 library.

ACKNOWLEDGMENTS

We are thankful to the operating staff of the BARC-TIFR Pelletron Accelerator for smooth operation of the accelerator during the experiment. We acknowledge the support of the Department of Atomic Energy, Government of India, under Project Identification No. RTI 4002. R.G. thanks G. K. Prajapati for useful discussions. A.D.-T. is supported by the STFC Consolidated Grant No. ST/P005314/1.

APPENDIX: APPLICABILITY OF SURROGATE RATIO METHOD

Detailed calculations have been carried out for the present reaction systems to verify the three conditions put up by Chiba *et al.* [15,16] (as mentioned in Sec. II) for the applicability of

the surrogate ratio method to determine the neutron-induced capture cross sections, as described below.

1. Equivalence of spin distribution

To find the equivalence of the spin distributions (σ_J versus J) of two compound nuclei $^{58}\text{Co}^*$ and $^{61}\text{Ni}^*$ which are populated by surrogate reactions $^{56}\text{Fe}(^6\text{Li}, \alpha)^{58}\text{Co}^*$ and $^{59}\text{Co}(^6\text{Li}, \alpha)^{61}\text{Ni}^*$, respectively, and used in the SRM, the incomplete fusion cross sections have been calculated at beam energies 35.9 and 40.5 MeV using the three-body classical dynamical model code PLATYPUS [26–28]. Potential parameters (projectile-target, i.e., $^6\text{Li} + ^{56}\text{Fe}/^{59}\text{Co}$ and fragment-target, i.e., $d + \text{target}$ and $\alpha + \text{target}$) used as inputs to this code are taken from the global Broglia-Winther parametrization [29]. The fragment-fragment, i.e., $d + \alpha$ interaction potential parameters are taken from Ref. [30]. The key inputs of the $d + \alpha$ system for the PLATYPUS calculations (e.g., those determining the intrinsic probability density function of the ^6Li ground state) are given in Ref. [31]. The calculated results for incomplete fusion/transfer cross sections for the two systems have been compared in Fig. 10.

It can be observed that the spin distributions for both the systems are very close to each other. Hence, the above exercise suggests that the spin distribution (σ_J versus J) in two compound nuclei $^{58}\text{Co}^*$ and $^{61}\text{Ni}^*$ which are populated by surrogate reactions $^{56}\text{Fe}(^6\text{Li}, \alpha)$ and $^{59}\text{Co}(^6\text{Li}, \alpha)$, respectively, are equivalent.

2. Spin population in neutron-induced and surrogate reactions

The average spin angular momenta $\langle J \rangle$ populated for the incomplete fusion/transfer reactions have been calculated from the spin distribution shown in Fig. 10 and found to be

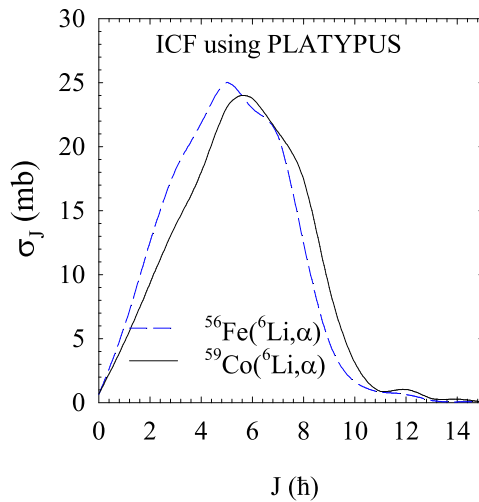


FIG. 10. Cross sections for incomplete fusion/transfer corresponding to the capture of deuteron fragment by the target in the reactions $^{56}\text{Fe}(^6\text{Li}, \alpha)^{58}\text{Co}^*$ (dashed line) and $^{59}\text{Co}(^6\text{Li}, \alpha)^{61}\text{Ni}^*$ (solid line) at beam energies 35.9 and 40.5 MeV, respectively, calculated using the three-body classical dynamical model code PLATYPUS.

5.1 and $5.6\hbar$ for two systems, respectively. However, the average spins populated in compound nuclei $^{58}\text{Co}^*$ and $^{61}\text{Ni}^*$ in neutron-induced reactions $n + ^{57}\text{Co}$ and $n + ^{60}\text{Ni}$ for neutron energies corresponding to the peaks of excitation energies of CN populated in surrogate reactions $^{56}\text{Fe}(^6\text{Li}, \alpha)^{58}\text{Co}^*$ and $^{59}\text{Co}(^6\text{Li}, \alpha)^{61}\text{Ni}^*$ calculated using the statistical model code PACE4 are found to be ≈ 4 and $5\hbar$, respectively. So the differences in spin values between neutron-induced and corresponding surrogate reactions used in the present work are much less than $10\hbar$, thus satisfying the second condition of Chiba *et al.* [15,16].

3. J^π -by- J^π convergence

The statistical model code PACE4 was used to calculate (i) the decay branching ratios of various spin (J) states of the compound nuclei $^{58}\text{Co}^*$ and $^{61}\text{Ni}^*$ formed in the surrogate reactions $^{56}\text{Fe}(^6\text{Li}, \alpha)^{58}\text{Co}^*$ and $^{59}\text{Co}(^6\text{Li}, \alpha)^{61}\text{Ni}^*$,

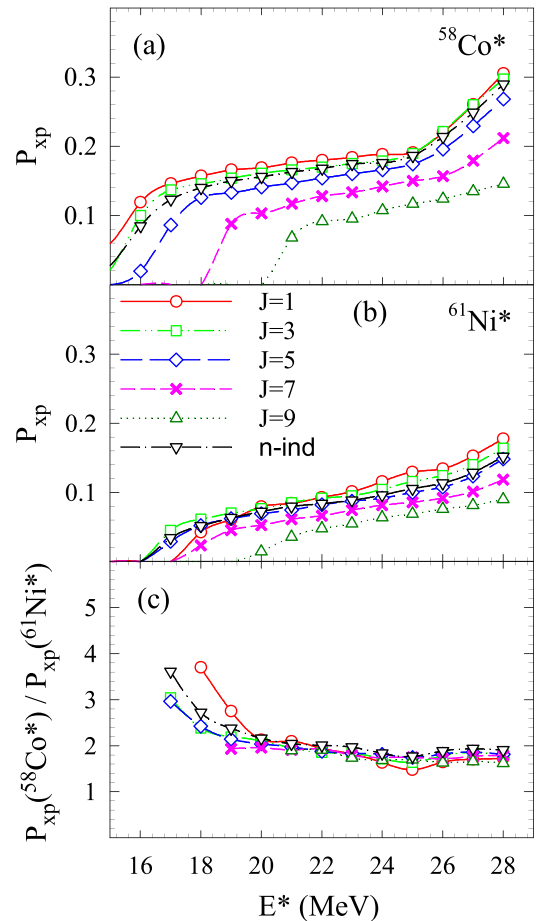


FIG. 11. (a) The decay branching ratios P_{xp} of various spin (J) states of compound nucleus $^{58}\text{Co}^*$ formed in the surrogate reaction $^{56}\text{Fe}(^6\text{Li}, \alpha)^{58}\text{Co}^*$ and of corresponding n -induced reaction $n + ^{57}\text{Co}$, as a function of excitation energy (E^*). (b) Same as (a) but for compound nucleus $^{61}\text{Ni}^*$ formed in the surrogate reaction $^{59}\text{Co}(^6\text{Li}, \alpha)^{61}\text{Ni}^*$ and of corresponding n -induced reaction $n + ^{60}\text{Ni}$. (c) Ratio of P_{xp} of various spin (J) states of compound nuclei $^{58}\text{Co}^*$ to $^{61}\text{Ni}^*$ compared with the ones corresponding to the n -induced reactions, as a function of E^* .

respectively, and (ii) the branching ratios of the corresponding neutron-induced reactions, i.e., $n + ^{57}\text{Co}$ and $n + ^{60}\text{Ni}$. The decay probabilities P_{xp} for compound nuclei $^{58}\text{Co}^*$ and $^{61}\text{Ni}^*$ decaying to xp (proton emission) channels from various J states have been calculated up to $J = 9$ for different excitation energies in the range of $E^* = 15\text{--}28$ MeV as shown in Figs. 11(a) and 11(b), respectively. It can be seen that P_{xp} has significant J dependence for each of the compound nuclei $^{58}\text{Co}^*$ and $^{61}\text{Ni}^*$ for the entire excitation energy range in the present study. So the standard Weisskopf-Ewing approximation which assumes that decay branching ratios are independent of spin-parity states, is not fulfilled in the above case and the absolute surrogate method is not useful. However, the ratio of decay probabilities $P_{xp}(^{58}\text{Co}^*)/P_{xp}(^{61}\text{Ni}^*)$ as shown in Fig. 11(c) shows a weak J dependence, where a good convergence is observed among all J distributions. The ratios of the proton emission probabilities [$\sigma^{(n,xp)}/\sigma^{(n,\text{total})}$]

of $^{58}\text{Co}^*$ to that of $^{61}\text{Ni}^*$ populated by neutron capture reactions are also shown in Fig. 11 as black dash-dotted line (with down-triangles). It can be observed that all the curves in Fig. 11(c) appear to converge to the black dash-dotted line within the deviation of 8–19% in the excitation energy range of $E^* = 19\text{--}28$ MeV. It may be mentioned here that the most probable J values populated in two surrogate reactions are around $5\hbar$ (see Fig. 10) corresponding to which the percentage deviation in the probability ratios is found to be up to 10%. Hence, in case of the surrogate ratio method the “ J^π -by- J^π convergence” condition of Chiba *et al.* (known as weak Weisskopf-Ewing approximation) is satisfied for the present systems in the excitation energy range of $E^* = 19\text{--}28$ MeV and the calculations suggest that the SRM would give a reasonable estimate of the $^{57}\text{Co}(n, xp)$ reaction cross sections for the corresponding equivalent neutron energies within the theoretical systematic uncertainties of 8–19%.

-
- [1] Report summary of European facility for innovative reactor and transmutation neutron data (2013), Belgium, <https://cordis.europa.eu/project/rcn/88553/reporting/en>.
- [2] H. Iida, V. Khripunov, L. Petrizzi, and G. Federici, Technical Report G 73 DDD 2W 0.2, Nuclear Analysis Group, ITER Naka & Garching Joint Work Sites (2004).
- [3] M. R. Gilbert, S. L. Dudarev, S. Zheng, L. W. Packer, and J.-C. Sublet, *Nucl. Fusion* **52**, 083019 (2012).
- [4] S. Fetter, E. T. Cheng, and F. M. Mann, *Fusion Eng. Des.* **6**, 123 (1988).
- [5] R. A. Forrest, *Fusion Eng. Des.* **81**, 2143 (2006).
- [6] R. A. Forrest, A. Tabasso, C. Danani, S. Jakhar, and A. K. Shaw, *Handbook of Activation Data Calculated Using EASY-2007* (EURATOM/UKAEA Fusion Association, Culham Science Centre, Abingdon, UK, 2009).
- [7] J. M. A. Plompen, D. Smith, P. Reimer, S. Qaim, V. Semkova, F. Cserpák, V. Avrigeanu, and S. Sudar, *J. Nucl. Sci. Technol.* **39**, 192 (2002).
- [8] B. Pandey, V. V. Desai, S. V. Suryanarayana, B. K. Nayak, A. Saxena, E. T. Mirgule, S. Santra, K. Mahata, R. Makawana, M. Abhangi, T. K. Basu, C. V. S. Rao, S. Jakhar, S. Vala, B. Sarkar, H. M. Agrawal, G. Kaur, P. M. Prajapati, A. Pal, D. Sarkar, and A. Kundu, *Phys. Rev. C* **93**, 021602(R) (2016).
- [9] J. Pandey, B. Pandey, A. Pal, S. V. Suryanarayana, S. Santra, B. K. Nayak, E. T. Mirgule, A. Saxena, D. Chattopadhyay, A. Kundu *et al.*, *Phys. Rev. C* **99**, 014611 (2019).
- [10] R. Gandhi, B. K. Nayak, S. V. Suryanarayana, A. Pal, G. Mohanto, S. De, A. Parihari, A. Kundu, P. C. Rout, S. Santra *et al.*, *Phys. Rev. C* **100**, 054613 (2019).
- [11] A. Gavron, *Phys. Rev. C* **21**, 230 (1980).
- [12] K. Shibata, O. Iwamoto, T. Nakagawa, N. Iwamoto, A. Ichihara, S. Kunieda, S. Chiba, K. Furutaka, N. Otuka, T. Ohsawa *et al.*, *J. Nucl. Sci. Technol.* **48**, 1 (2011).
- [13] EXFOR Data Library, <https://www-nds.iaea.org/exfor/exfor.htm>.
- [14] A. Koning and D. Rochman, *Nucl. Data Sheets* **113**, 2841 (2012).
- [15] S. Chiba and O. Iwamoto, *Phys. Rev. C* **81**, 044604 (2010).
- [16] S. Chiba, O. Iwamoto, and Y. Aritomo, *Phys. Rev. C* **84**, 054602 (2011).
- [17] A. J. M. Plompen, O. Cabellos, and C. D. S. Jean, *Eur. Phys. J. A* **56**, 181 (2020).
- [18] W. Hauser and H. Feshbach, *Phys. Rev.* **87**, 366 (1952).
- [19] R. Capote, M. Herman, P. Obložinsky, P. G. Young, S. Goriely, T. Belgia, A. V. Ignatyuk, A. J. Koning, S. Hilaire, V. A. Plujko *et al.*, *Nucl. Data Sheets* **110**, 3107 (2009).
- [20] A. Koning and J. Delaroche, *Nucl. Phys. A* **713**, 231 (2003).
- [21] A. Gilbert and A. G. W. Cameron, *Can. J. Phys.* **43**, 1446 (1965).
- [22] W. Dilg, W. Schantl, H. Vonach, and M. Uhl, *Nucl. Phys. A* **217**, 269 (1973).
- [23] A. V. Ignatyuk, J. L. Weil, S. Raman, and S. Kahane, *Phys. Rev. C* **47**, 1504 (1993).
- [24] S. Goriely, S. Hilaire, and A. J. Koning, *Phys. Rev. C* **78**, 064307 (2008).
- [25] S. Hilaire, M. Girod, S. Goriely, and A. J. Koning, *Phys. Rev. C* **86**, 064317 (2012).
- [26] A. Diaz-Torres, *Comput. Phys. Commun.* **182**, 1100 (2011).
- [27] A. Diaz-Torres, D. J. Hinde, J. A. Tostevin, M. Dasgupta, and L. R. Gasques, *Phys. Rev. Lett.* **98**, 152701 (2007).
- [28] A. Diaz-Torres, *J. Phys. G: Nucl. Part. Phys.* **37**, 075109 (2010).
- [29] W. Reisdorf, *J. Phys. G: Nucl. Part. Phys.* **20**, 1297 (1994).
- [30] A. Diaz-Torres, I. J. Thompson, and C. Beck, *Phys. Rev. C* **68**, 044607 (2003).
- [31] A. Diaz-Torres and D. Quraishi, *Phys. Rev. C* **97**, 024611 (2018).